35th Annual International Conference of the IEEE EMBS
Osaka, Japan, 3 - 7 July, 2013

The feasibility study on 3-dimensional fluorescent x-ray computed tomography using the pinhole effect for biomedical applications

Naoki Sunaguchi, Tetsuya Yuasa, *Senior Member, IEEE*, Kazuyuki Hyodo, and Tsutomu Zeniya

Abstract— **We propose a 3-dimensional fluorescent x-ray computed tomography (CT) pinhole collimator, aimed at providing molecular imaging with quantifiable measures and sub-millimeter spatial resolution. In this study, we demonstrate the feasibility of this concept and investigate imaging properties such as spatial resolution, contrast resolution and quantifiable measures, by imaging physical phantoms using a preliminary imaging system developed with monochromatic synchrotron x rays constructed at the BLNE-7A experimental line at KEK, Japan.**

I. Introduction

Fluorescent x-ray computed tomography (FXCT), which combines x-ray fluorescence analysis and tomographic reconstruction algorithms, delineates the spatial distribution of imaging agents within samples with high sensitivity, reproducible and quantifiable measures, and at high spatial resolutions, in a non-destructive and non-invasive manner [1-3]. FXCT has been a vital tool in both material and biomedical sciences [4-6]. Molecular imaging using a non-radioactive imaging-agent, such as iodine, is also of potential use in medicine and pharmacology, where the visualization of various disease processes in small animals is used to investigate the cause, diagnosis and therapy of diseases from the characteristics and behavior of imaging agents in the subject. Studies using mice and rats as animal models have become important in many areas, such in molecular biology, toxicology, and drug discovery research. Hypotheses regarding the onset of disease and the effectiveness of treatment can be tested with animals before progressing to human studies. As a consequence of utilizing small animals, imaging modalities such as positron emission tomography (PET) or single photon emission computed tomography (SPECT) have been developed for small animals studies [7, 8]. However, such diagnostic imaging modalities still suffer from insufficient spatial resolution. In addition, the radioactive imaging contrast agents are required. Therefore, the invention of a novel molecular imaging technique using non-radioactive imaging agents with high-contrast and high spatial resolutions would have a positive clinical impact.

So far, we have developed two types of FXCT with sub-millimeter resolution: one based on pencil-beam geometry, and the other on sheet-beam geometry. The former acquires a set of projections by translational and rotational scans using pencil-beam geometry [1, 2]. Unfortunately, it takes an enormous amount of acquisition time to acquire a 3-dimensional tomographic image as the pencil beam method collects sequential data. In order to overcome this difficulty, a parallel data acquisition scheme has been proposed using an incident-sheet beam using a linear detectors array [3]. We demonstrated the efficacy using a preliminary simulated system. However, although the system requires a linear array of energy-resolving detectors with fine pixel size, such detector arrays have progressively been technically refined; unfortunately the spatial resolution has not yet reached sub-millimeter dimensions. In this letter, we propose a 3-dimensional FXCT imaging method using a pinhole methodology which utilizes an ordinary CCD (charge coupled device) camera without energy resolution.

Naoki Sunaguchi is with the Graduate School of Engineering, Gunma University, Kiryu, Gunma 376-8515, Japan (corresponding author to provide e-mail: sunaguchi@gunma-u.ac.jp).

Tetsuya Yuasa is with the Faculty of Engineering, Yamagata University, Yonezawa, Yamagata, 992-8510, Japan (e-mail: yuasa@yz.yamagata-u.ac.jp).

Kazuyuki Hyodo is with the Institute of Materials Structure Science, KEK, Tsukuba, Ibaraki 305-0801, Japan (e-mail: kazuyuki.hyodo@kek.jp).

Tsutomu Zeniya is with the Department of Investigative Radiology, National Cerebral and Cardiovascular Center Research Institute, Suita, Osaka 565-8565, Japan (e-mail: zeniya@ri.ncvc.go.jp).

II. Measurement process in fluorescent x-ray CT imaging

Fig. 1 shows a schematic diagram of the proposed imaging geometry. An incident monochromatic volumetric beam, with photon fluxes parallel to one another are linearly polarized within a horizontal plane, impinging and covering the object. Imaging agents, such as iodine, are thus excited and isotropically emit x-ray fluorescent photons on de-excitation. A thin W plate with a pinhole is placed between the object and the CCD camera, such that the plate surface and the detective surface are parallel to the beam propagation. Only fluorescent photons passing through the pinhole are detected by the CCD, as discussed below. The projection acquisition is repeated while rotating the object over 180 degrees.

The modeling process proceeded as follows. First, we modeled the measurement process for reconstruction using Fig. 1. Consider events relating to a single ray along the volumetric beam. The points P and R represent the intersections of the ray with the object. Pay attention to a point Q on the line segment $\overline{PR}$. Let a point S be the intersection of the line, connecting point Q with point Π of the pinhole center, with the object. Regarding the measurement by the CCD along path $P \to Q \to S$ in Fig. 1, the measurement process is divided into the following three steps: **Step 1)** The incident radiation travels from P to Q while undergoing attenuation by the object. The interaction for the single ray at point Q is given by $I_1(Q) = I_0 \exp\left(-\int_{\overline{PQ}} \mu_I dl\right)$, where I_0 and $\mu_I(\boldsymbol{r})$ are the intensity of the incident beam and the 3-D map of the object consisting of the linear attenuation coefficient for the energy of the incident x ray, respectively. **Step 2)** The fluorescent x-ray fluxes are emitted isotropically at point Q in a quantity proportional to the product of the incident intensity $I_1(Q)$ and

978-1-4577-0216-7/13/$26.00 ©2013 IEEE

the concentration map of imaging agents $d(Q)$ at Q. The fluorescent photon fluxes from point Q is given by $I_2(Q) = \mu_{ph}\omega I_1(Q)d(Q)\Delta v_Q$, where μ_{ph}, ω, and Δv_Q are the photoelectric linear attenuation coefficient of the imaging agent material, the fluorescent yield of agent material, and the infinitesimal volume around point Q, respectively. **Step 3)** From the total fluorescent photons emitted at point Q, only the fluorescent photons traveling towards the pinhole are detected by the CCD, where the camera receives information regarding attenuation measurements by the object during flight. The flux rate reaching the detection plane is given by $I_3(Q) = I_2(Q)(\Omega(Q)/4\pi)\exp\left(-\int_{\overline{QS}} \mu_F dl\right)$ under the approximation that the pinhole area is sufficiently small and the W plate is sufficiently thin, where $\Omega(Q)$ and $\mu_F(\boldsymbol{r})$ are the solid angle from point Q to the pinhole and the 3-D map of the object's linear attenuation coefficient for the fluorescent x ray energy, respectively. As a result, the CCD detective elements within the projected circle of the pinhole from point Q to the detective surface evenly acquire the fluorescent flux $I_3(Q) = C(Q)d(Q)$, where

$$C(Q) = \mu_{ph}\omega I_0(\Omega(Q)/4\pi)\exp\left(-\int_{\overline{PQ}} \mu_I dl\right)\exp\left(-\int_{\overline{QS}} \mu_F dl\right)\Delta v_Q . \quad (1)$$

Note that $C(Q)$ can be calculated if the imaging setup geometry and the 3-D maps, μ_I and μ_F, of the object are previously known. We did not consider scatter components in this preliminary research.

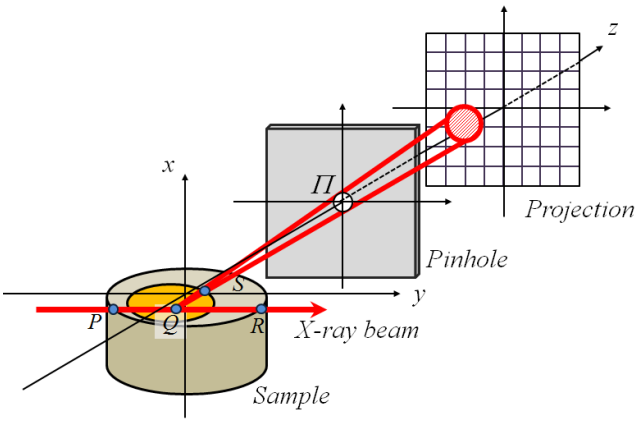

Figure 1. Schematic diagram of the proposed imaging geometry: The system is composed of a rotation stage for object placement, a pinhole set perpendicularly to the direction of the incident x-ray beam and a CCD camera set behind the pinhole. Fluorescent photons emitted within an object pass through the pinhole and are subsequently projected onto the CCD camera imaging plane.

III. Three-dimensional CT reconstruction

For the reconstruction process, the object space is discretized to 3-D voxels. Three 3-D arrays d_j, μ_{Ij} and μ_{Fj} are prepared, where j ($1 \le j \le N$) is the index identifying the voxel; d_j is unknown, while μ_{Ij}, and μ_{Fj} are known. Note that in the reconstruction scheme the object is fixed and the imaging components are rotated around the object, although in reality only the object is rotated. The introduction of indices i ($1 \le i \le M$) and k ($1 \le k \le L$) identify the detective element and the projection angle, respectively. Consider the signal intensity ski acquired by the ith detector at the kth projection (Fig. 2). First, let us assume that the cone $v^k{}_i$ whose cross section is the pinhole and its apex is the ith detector. Next, we define $V^k{}_i$ as the set of indices denoting voxels which are contained within cone $v^k{}_i$. The ith detector simultaneously acquires the fluorescent photons from the voxels within cone $v^k{}_i$. Therefore,

$$s^k{}_i = \sum_{j \in V^k{}_i} C^k{}_{ij} d_j \ (1 \le i \le M,\ 1 \le k \le L), \quad (2)$$

where $C^k{}_{ij}$ corresponds to $C(Q)$ in the case where point Q is the jth voxel for the ith detective element at the kth projection; this can be previously calculated using (1) if the imaging geometry and the 3-D maps of μ_I and μ_F of the object are known. As a result, we obtain a system of ML linear equations. Finally, we obtain L matrix equations $\boldsymbol{s}^k = \boldsymbol{C}^k\boldsymbol{d}$ ($1 \le k \le L$) by arranging (2), where $\boldsymbol{s}^k = (s^k{}_1, s^k{}_2, \ldots, s^k{}_M)^T$, $\boldsymbol{d} = (d_1, d_2, \ldots, d_N)^T$, and

$$C^k = \begin{pmatrix} C^k{}_{11} & C^k{}_{12} & \cdots & C^k{}_{1N} \\ C^k{}_{21} & \ddots & & C^k{}_{2N} \\ \vdots & & \ddots & \vdots \\ C^k{}_{M1} & C^k{}_{M2} & \cdots & C^k{}_{MN} \end{pmatrix} \quad \text{for } C^k{}_{ij} = 0 \text{ if } j \notin V^k{}_i.$$

We solve these matrix equations using OS-EM (ordered subsets - expectation maximization) algorithm [9].

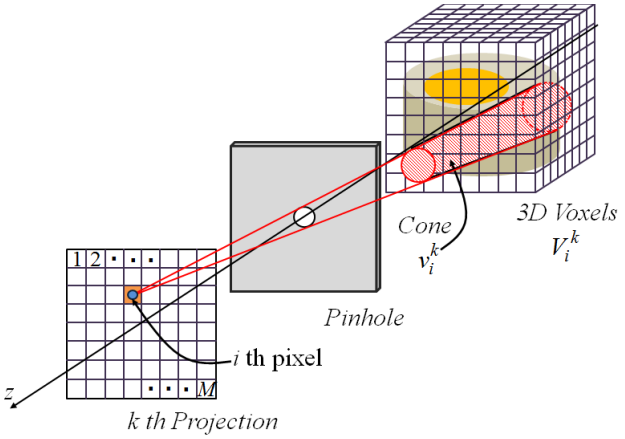

Figure 2. Reconstruction scheme: $v^k{}_i$ is the cone constructed from the apex of the ith detector and the pinhole cross section. $V^k{}_i$ is the set of indices denoting voxels which are contained within cone $v^k{}_i$. The ith detector simultaneously acquires the fluorescent photons from the voxels within cone $v^k{}_i$.

IV. Imaging experiment

In order to prove the concept of this imaging protocol, we constructed a preliminary imaging system at the BLNE-7A bending-magnet beamline (6.5 GeV) at KEK, Japan. The photon flux rate in front of the object was approximately 9.3×107 photons/mm^2/s for a beam current of 40 mA. The FXCT system consisted of a silicon (220) double crystal monochromator to tune the incident energy to 33.4 keV which is just above the iodine K-edge of 33.2 keV, an x-ray slit system to shape a volumetric beam of 35 × 5 mm^2, a rotational table for object-positioning, a 500 μm-thick W plate with a pinhole of 100 μm in diameter, and a CCD camera with 500 × 332 elements of 100 × 100 μm^2 in pixel-size to detect emitted fluorescent photons. The CCD and the rotational stage were controlled by a PC. The distance between the center of rotation and the W plate, and between the W plate and the

CCD detective surface were 45 mm and 45 mm, respectively. The linear attenuation coefficients of acryl for the incident beam energy (33.4 keV), μ_I, and the fluorescent one (28.3 keV), μ_F, were set to 0.0316 mm^{-1} and 0.0385 mm^{-1}, respectively.

A. Evaluation of spatial resolution, contrast resolution and quantifiable measures

Firstly, we evaluated the contrast resolution and its quantifiable measures by imaging a physical phantom. The acrylic cylindrical phantom was 10 mm in diameter and included three axial channels of 3 mm in diameter, filled with iodine at three different concentrations. The rotational step was one degree over 180 degrees; the number of projections L was 180. The measurement time for a single projection was 2.5 minutes. Fig. 3 (a) and (b) show an FXCT image and 3-D FXCT image of the physical phantom filled with an iodine solution with concentrations equivalent to 1.85 mg/ml, 3.7 mg/ml, and 7.4 mg/ml, respectively. Three circles corresponding to the regions including the iodine solution are successfully delineated. Fig. 3 (c) shows the differential profile at the white line drawn in Fig. 3 (a). The in-plane spatial resolution defined by the FWHM of the differential profile peak was approximately 300 μm. We imaged the phantom while changing the iodine concentrations, and then obtained the average reconstructed values for the regions of interest and added the iodine values to the reconstructed images. Fig. 3 (d) shows the relationship between the average reconstructed values and the actual iodine concentrations, which demonstrates a satisfactory linear relationship. Error bars of each plot show the standard deviation of noise on reconstructed iodine signals. The dotted line represents the standard deviation of the background noise in the reconstructed images. The minimum detectable iodine concentration, which can be calculated from the intersection of the calibration line and the dotted line representing background noise, is approximately 1 mg/ml.

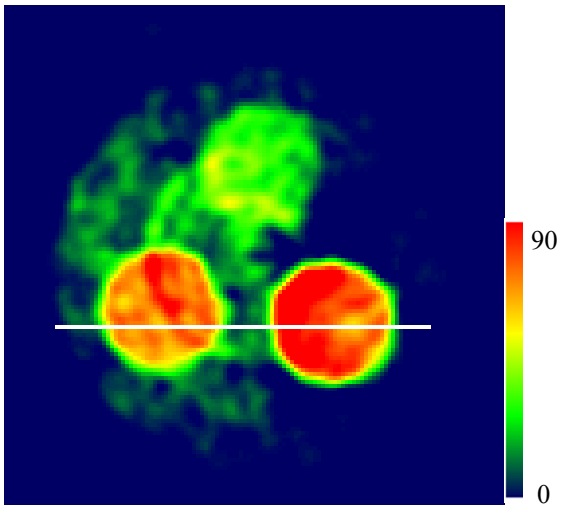

(a)

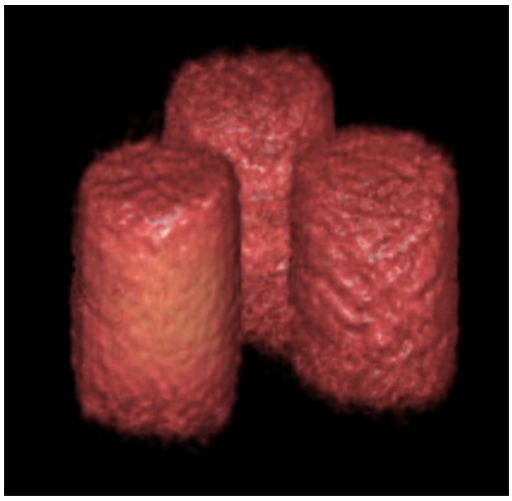

(b)

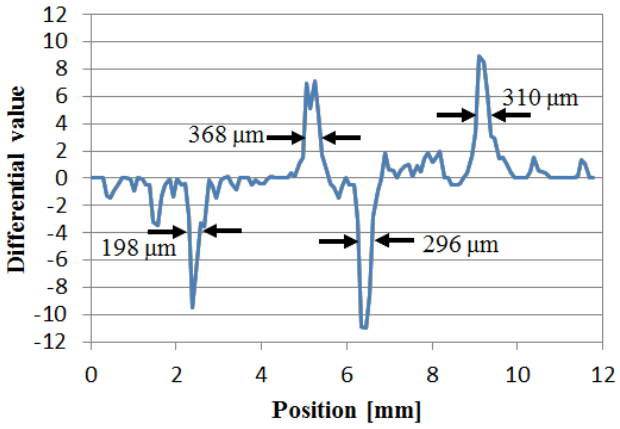

(c)

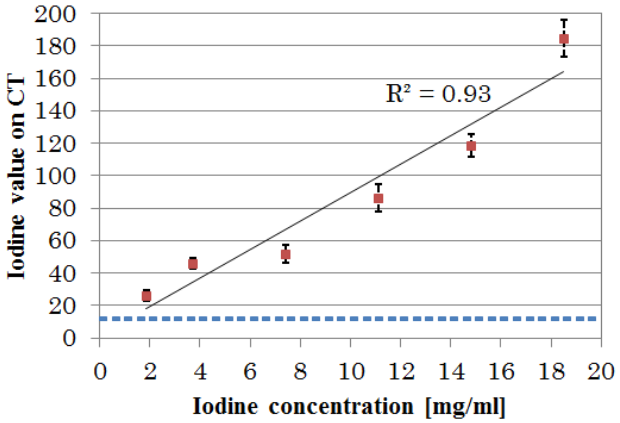

(d)

Figure 3. The experimental results from the 3-D FXCT system. The acrylic cylindrical phantom which was 10 mm in diameter and included three axial channels of 3 mm in diameter, filled with iodine at three different concentrations, is measured: (a) an FXCT image of the physical phantom filled with iodine solution at 1.85 mg/ml, 3.7 mg/ml, and 7.4 mg/ml, (b) 3-D FXCT volume rendering image, (c) differential profile at the white line drawn in (a), and (d) the relationship between the average reconstructed values and the actual iodine concentrations.

B. *Evaluation of spatial resolution in vertical direction*

Next, we imaged a hand-made physical phantom to evaluate the vertical spatial resolution. The phantom was an acrylic screw with a 200-to-300-μm-thick Polyester thread wound along the groove after it was first dipped in iodine solution and then dried out (Fig. 4(a)). Fig. 4(b) shows the 3-D FXCT image. The 200-to-300-μm thick thread was satisfactorily delineated.

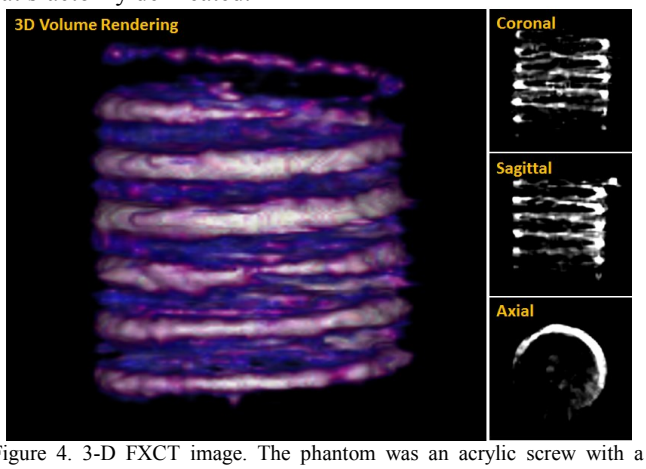

Figure 4. 3-D FXCT image. The phantom was an acrylic screw with a 200-to-300-μm-thick Polyester thread wound along the groove after first being dipped in an iodine solution and then dried out

V. Conclusion

In this research, we demonstrated the first 3-D FXCT image at a spatial resolution of approximately 300 μm using a CCD camera having no energy resolution, although conventional methods have only obtained 2-D cross-sections. In theory, the spatial resolution with a pinhole of 100 μm diameter is approximately 200 μm [10]. We consider that the spatial resolution improve to incorporate a point spread function based on the system into the reconstruction scheme. As this research was a feasibility study, we neglected the influence of Compton scatter. Using the two projection images acquired just above and below the K-edge, we can estimate the Compton scatter components, leading to the improvement of the contrast resolution. Finally, the measurement time is still long. We will adopt the multi-pinholes to improve the efficiency of data acquisition.

Acknowledgment

The authors would like to sincerely thank Prof. M. Ando and Dr. K. Hirano for the loan of the CCD cameras. This research was partially supported by a Grant-In-Aid for Scientific Research (#20500385, #23602002, #24.1109) from the Japanese Ministry of Education, Science and Culture, and performed under the auspices of KEK (2012G002, 2012PF05)

References

[1] J.P. Hogan, "Fluorescent computer tomography: a model for correction of X-ray absorption," *IEEE Trans Nucl. Sci.*, Vol. 38, pp. 1721–1727 1991.

[2] T. Yuasa, M. Akiba, T. Takeda, M. Kazama, A. Hoshino, Y. Watanabe, K. Hyodo, F.A. Dilmanian, T. Akatsuka, Y. Itai, "Reconstruction method for fluorescent X-ray computed tomography by least-squares method using singular value decomposition," *IEEE Trans. Nucl. Sci.*, Vol. 44, pp. 54–64 1997.

[3] Q. Huo, T. Yuasa, T. Akatsuka, T. Takeda, J. Wu, Thet-Thet-Lwin, K. Hyodo, F.A. Dilmanian, "Sheet-beam geometry for in vivo fluorescent x-ray computed tomography: proof-of-concept experiment in molecular imaging," *Optics Lett.*, Vol. 33, pp. 2494–2496 2008.

[4] T. Takeda, J. Wu, Thet-Thet-Lwin, Q. Huo, T. Yuasa, K. Hyodo, F.A. Dilmanian, T. Akatsuka, "X-ray fluorescent CT imaging of cerebral uptake of stable-iodine perfusion agent iodoamphetamine analog IMP in mice," *J. Synchrotron Rad.*, Vol. 16, pp. 57–62, 2009.

[5] Thet-Thet-Lwin, T. Takeda, J. Wu, Q. Huo, T. Yuasa, K. Hyodo, T. Akatsuka, "Visualization of age-dependent myocardial metabolic impairment in cardiomyopathic model hamster obtained by fluorescent X-ray computed tomography using I-127 BMIPP," *J. Synchrotron Rad.*, Vol. 15 pp. 528–531 2008.

[6] C. Schroer, "Reconstructing x-ray fluorescence microtomograms," *Appl. Phys. Lett.*, Vol. 79, pp. 1912–1914 2001.

[7] F. van der Have, B. Vastenhouw, R. M. Ramakers, W. Branderhorst, J. O. Krah, C. Ji, S. Staelens, F. J. Beekman, "U-SPECT-II: An Ultra-High-Resolution Device for Molecular Small-Animal Imaging," *J. Nucl. Med.*, Vol. 50, pp. 599–605 2009.

[8] K. Magota, N. Kubo, Y. Kuge, K. I. Nishijima, S. Zhao, N. Tamaki, "Performance characterization of the Inveon preclinical small-animal PET/SPECT/CT system for multimodality imaging," *Eur. J. Nucl. Med.*, Vol. 38, pp. 742–752 2011.

[9] H. M. Hudson, R. S. Larkin, "Accelerated image reconstruction using ordered subsets of projection data," *IEEE Trans. Med. Imag.*, Vol. 13 pp. 601–609 1994.

[10] Anger HO, Instrumentation in Nuclear Medicine, Academic Press, New York, 1967, p. 485.